

Heat transfer optimization of UO_2 -Mo fuel using genetic algorithms

Jacob P. Gorton,* Joel L. McDuffee, Patrick L. Snarr, Christian M. Petrie, Andrew T. Nelson

Oak Ridge National Laboratory, PO Box 2008, Oak Ridge, TN 37831, USA

ABSTRACT

Two genetic algorithm (GA) methods were applied to thermal finite element models to optimize the heat transfer efficacy of a UO_2 -Mo composite fuel pellet with typical pressurized water reactor fuel geometry. Mo additions to UO_2 have been shown to increase the thermal conductivity, thus reducing centerline temperatures and temperature gradients. Previous studies evaluated uniformly dispersed Mo or continuous Mo internal geometries (e.g., fins, plates, discs) that were selected using engineering intuition. The current study uses two different implementations of the same GA to optimize Mo placement and minimize the fuel temperature with the only constraint being a maximum 10% Mo volume fraction. One approach superimposed Mo line elements onto the monolithic UO_2 pellet model, and the other converted entire UO_2 volume elements to Mo. The former method generated 1D heat transfer connections between nodes, whereas the latter method allowed for the formation of 3D structures. Features of the optimal fuel design produced by the GAs included dispersed Mo near the centerline that shifted the peak fuel temperature outward by 0.6 mm, Mo chains in the high-heat-flux region in the mid-to-outer radial zone, and a large continuous structure that spanned the full radius and height of the pellet and accounted for 87.7% of the total Mo in the pellet. Analysis of this design indicates that the optimal Mo configuration is a balance between creating continuous heat transfer pathways and optimally dispersing Mo to minimize the heat transfer distance through UO_2 . This architecture ultimately produced an effective thermal conductivity of 11.3 W/m·K under the assumed boundary conditions. This result is higher than any previous values from the literature. Potential fabrication methods and challenges are discussed in addition to the implications on fuel performance.

Keywords: Nuclear fuel, Composite fuels, Thermal conductivity, Heuristic algorithms

1. Introduction

Composite fuels comprising UO_2 and Mo are being considered for nuclear reactors to improve heat transfer relative to monolithic UO_2 pellets and to potentially enhance reactor performance and safety. Key properties of Mo that make it a suitable material for admixture with UO_2 and for enhancing heat transfer efficiency include chemical compatibility with UO_2 , a comparable melting point to UO_2 , and a high thermal conductivity [1]. Increasing the fuel's thermal conductivity has numerous benefits for fuel performance as well as reactor performance and safety, owing to a reduction in fuel temperatures, stored energy, and temperature gradients across the fuel pellet radius. Reductions in fuel temperature and stored energy from enhanced thermal conductivity provide additional thermal margin during short-term accidents in pressurized water reactors (PWRs) [2]. Pellet-cladding interactions and fuel cracking could be reduced because of lower fuel temperatures and thermal expansion [3], or larger fuel pellets could be

1 loaded into the same cladding diameter to increase the fissile inventory without increasing the centerline
2 temperature. Fission product retention is enhanced by reductions in fuel temperatures and temperature
3 gradients owing to reduced fission product mobilities [4] and by burst release of gas caused by fuel
4 cracking. Less fission gas released during normal operation could reduce the probability that the fuel rod
5 bursts during loss-of-coolant accidents caused by the reduced rod internal pressure, which may support
6 discharge burnup extensions [5]. Each of these performance benefits could support reactor power uprates,
7 but numerous other factors would need to be considered [6, 7].

8 Historic attempts at improving the thermal conductivity of UO_2 by introducing a Mo secondary phase
9 focused on basic methods of composite fabrication. Powder feedstocks of UO_2 and Mo are combined via
10 various means, pressed into pellets, and sintered at a high temperature [1, 8, 9]. Despite variations in the
11 synthesis route used [8], the resulting microstructure consists of Mo secondary phases dispersed in a UO_2
12 matrix. Provided fabrication has not induced cracks or gross heterogeneities in the microstructure, the
13 increased thermal conductivity of Mo compared with UO_2 will yield a composite with a higher thermal
14 conductivity.

15 Recent efforts have focused on gains enabled by a more sophisticated incorporation of the high thermal
16 conductivity phase using continuous Mo networks to enhance radial heat transfer. This result could be
17 achieved using additive manufacturing (AM) [10] or traditional processing methods [11]. Modeling
18 performed to analyze such optimized configurations of UO_2 -Mo fuels confirms that the bulk thermal
19 conductivity can vary greatly depending on the placement of Mo within the pellet, even when the volume
20 fraction of the Mo phase is held constant [12, 13]. However, the modeling studies performed to date are
21 generally constrained to a continuous Mo network with imposed geometries (e.g., fins, rods, discs) that
22 were selected based on engineering judgement of fabricability or simplicity.

23 This work seeks to optimize the UO_2 -Mo pellet configuration for maximum radial heat transfer using
24 finite element fuel pellet models and a Python-based genetic algorithm (GA) without any assumptions or
25 constraints on the geometric configuration of the Mo phase aside from limiting the total Mo volume
26 fraction. Two implementations of the GA were developed for this study. The first superimposes Mo line
27 elements over the 3D finite element mesh of the UO_2 fuel pellet. These line elements represent 1D heat
28 transfer connections between nodes in the mesh and are therefore incapable of producing 3D structures.
29 The second implementation swapped entire UO_2 elements (known as voxels) in the mesh with Mo
30 elements. Because of the 3D nature of this approach, insert structures as well as dispersed or continuous
31 Mo networks could be constructed. The generated designs may provide an opportunity for AM techniques
32 to fabricate these optimized fuels because precise placement of Mo will be needed to replicate their
33 performance. A cursory review of previous studies investigating UO_2 -Mo fuels and an introductory
34 background on GAs are provided in Section 2 of this article. Section 3 describes the specific
35 implementation of GA methods and other details of the approach for this heat transfer optimization study.
36 Results from both GA simulations are presented in Section 4 and are discussed in Section 5.

37 **2. Background**

38 **2.1. Review of previous UO_2 -Mo analyses**

39 The thermal conductivity of UO_2 -Mo composites have been investigated in numerous studies in which the
40 fuel form was fabricated [1, 8, 9, 11] or studied computationally [11, 14, 12, 13]. Kim et al. [9] used
41 conventional sintering methods to fabricate fuel pellets using various Mo contents (2%, 5%, and 10%
42 volume fraction), Mo particle sizes (300 nm–20 μm), and UO_2 granule sizes (165–850 μm). Kim et al.'s
43 study [9] shows that UO_2 -Mo pellets with continuous Mo networks had greater thermal conductivities

1 than those with dispersed networks and that higher degrees of Mo connectivity could be achieved with
2 300 nm Mo particles, UO₂ granules sized < 400 μm, and a pre-compaction theoretical density of 33%.
3 Buckley et al. [1] demonstrated a spark plasma sintering method for fabricating UO₂-Mo fuel with 5%
4 and 10% Mo volume fractions and with the Mo preferentially oriented in the radial direction. The
5 measured thermal conductivity of these fuel specimens was slightly less than those produced by Kim et
6 al. [9]; this discrepancy was attributed to the Mo phase being discontinuous. Finkeldei et al. [8] sintered
7 UO₂-Mo fuel using two separate UO₂ feedstock preparation methods. In the first method, ammonium
8 diuranate feedstock powder was calcined to UO₂ to mimic conventional UO₂ processing. Large UO₃
9 microsphere feedstock produced using a sol-gel process was calcined to UO₂ and high-energy milled in
10 the other method. In both cases, Mo powder was mixed with the UO₂, cold pressed, and sintered. The
11 resulting microstructures contained 5% and 10% Mo volume fractions, and variations were made using
12 fine (< 800 nm) and coarse (15–45 μm) Mo particles. The fuels fabricated from the sol-gel feedstock and
13 fine Mo powder were shown to have the highest thermal conductivity of all UO₂-Mo fuels with 5% and
14 10% Mo volume fractions described in this section of the current paper. The composite fuels with 10 vol
15 % Mo and 5 vol % Mo exhibited thermal conductivity enhancements of ~60%–100% and ~40%–75%,
16 respectively, depending on the temperature relative to monolithic UO₂ properties reported by Fink [15].

17 Lee et al. [11] sintered UO₂ pellets containing Mo microplates that were 70 μm in diameter and 2–3 μm
18 thick, with a total Mo volume fraction of 3%. The microplates were predominately oriented in the radial
19 direction, and thermal conductivities of the fabricated pellets were found to be roughly 50% greater than
20 that of monolithic UO₂ at temperatures from 800°C to 1,200°C. A portion of the pellet was then modeled
21 in COMSOL Multiphysics finite element software, and a sensitivity analysis was performed based on the
22 axial and azimuthal spacing between microplates and on the angle of the plates relative to the radial
23 direction. As the orientation of the microplates shifted toward vertical, the thermal conductivity of the
24 pellet model decreased drastically because heat transfer in a narrow cylinder is predominantly in the
25 radial direction. Reducing the axial spacing between the microplates and distributing them uniformly in
26 the azimuthal direction improved heat transfer. The COMSOL model predicted thermal conductivity in
27 good agreement with measurements for the fabricated pellet, especially when corrections were made
28 based on the angular distribution of microplates in the pellet.

29 Medvedev and Mariani [13] modeled two Mo insert structures embedded in the fuel pellet occupying
30 5 vol % using the BISON finite element code. The first design consisted of six fins that stretched the full
31 pellet height and protruded in the radial direction with equal azimuthal spacing, and the second consisted
32 of 50 μm thick Mo discs alternating with 950 μm thick UO₂ discs. The design with alternating UO₂ and
33 Mo demonstrated better heat transfer performance and lowered the peak fuel temperature from 1,950°C
34 for monolithic UO₂ to 955°C at a linear power of 500 W/cm. The bulk thermal conductivity for this
35 design can be calculated using Eq. (1):

$$k = \frac{\dot{Q}}{4\pi L \Delta T} , \quad (1)$$

36 where \dot{Q} is the total pellet power, L is the pellet length, and ΔT is the temperature gradient across the
37 pellet. Using the temperatures reported by Medvedev and Mariani and Eq. (1), the bulk thermal
38 conductivity of the alternating disc design is 7.86 W/m·K. Using the same linear heating rate, the
39 monolithic UO₂ pellet had a bulk thermal conductivity of 2.65 W/m·K. A follow-up study used
40 parametric analyses to optimize the finned insert by varying the number of fins, fin thickness, fin length,
41 insert thermal conductivity, and insert volume fraction. A temperature reduction of 1,200°C was achieved
42 using a linear heating rate of 500 W/cm [16].

1 Also using the BISON code, Gorton et al. [12] analyzed a Mo insert structure with an axially oriented
2 central rod connected to radially oriented discs. A sensitivity analysis was performed in which key
3 features of the geometry were varied, including the radius of the central rod, the number of radial discs,
4 the radius of each disc, and the thickness of the discs, to determine the effect on peak fuel temperature
5 and reactor cycle length. These features were varied under the constraint that the total Mo content was
6 fixed at 15 wt % (15.3 vol %). Although an increase in ^{235}U enrichment was needed to compensate for the
7 presence of Mo in the fuel, variations in the structure geometry had relatively little effect on the cycle
8 length. However, the heat transfer efficiency of the pellet was significantly affected by the insert
9 geometry. Out of 4,750 tested geometries, the temperature reduction relative to monolithic UO_2 ranged
10 from just 5.3% to 19.2%. An importance-ranking technique was implemented along with the sensitivity
11 analysis, showing that all four geometric parameters had a notable effect on the peak fuel temperature and
12 that the radius of the central rod was the most influential parameter. The results from this study suggest
13 that optimizing the Mo arrangement in a UO_2 -Mo fuel design is a balance between removing hotspots
14 (e.g., the centerline) and creating efficient heat transfer pathways.

15 Yan et al. [14] used Abaqus finite element software to develop 2D representative volume element models
16 of UO_2 -Mo microstructure and used machine learning methods to rapidly determine the thermal
17 conductivity based on various UO_2 microsphere sizes, distances between microspheres, porosity sizes and
18 densities, Mo volume fractions, and microcrack volume fractions. Model optimization showed that the
19 Mo volume fraction was the most important parameter for increasing thermal conductivity, but the best
20 UO_2 -Mo design at a fixed Mo volume fraction resulted from minimizing microcracks and retaining a
21 continuous distribution of Mo throughout the fuel. Microcrack propagation increased with increasing Mo
22 volume fraction, suggesting that incremental additions of Mo to the fuel provide diminishing returns.
23 Based on the optimization study, a UO_2 -Mo fuel pellet was fabricated with continuous 2 vol % Mo and no
24 microcracks. This pellet exhibited thermal conductivity 20% higher than that of monolithic UO_2 .

25 The thermal conductivity reported in these previous works varies significantly even at constant Mo
26 volume fractions. This variation may be caused by application of different fabrication methods, Mo
27 configurations, and boundary conditions used for measuring or simulating thermal conductivity. Defects
28 expected in the fuel from the different thermal expansion coefficients of UO_2 and Mo and any contact
29 resistance between the two phases were handled differently in the computational analyses, further
30 contributing to differences in model predictions. However, the sensitivity and optimization studies
31 detailed in this section showed that the placement of Mo within the fuel pellet can cause notable
32 variations in the peak fuel temperature at constant Mo volume fraction and identical boundary conditions.
33 From a reactor physics perspective, Mo is a strong resonance and thermal neutron absorber; thus, its
34 inclusion in the fuel will incur a penalty to the reactor cycle length [12]. Because of this neutronic penalty
35 and the evidence suggesting that the Mo configuration within the fuel pellet significantly affects thermal
36 performance, there is a clear need to identify the optimal arrangement of Mo that maximizes heat transfer
37 while minimizing the volume fraction of Mo in the pellet. Although a constant Mo volume fraction was
38 assumed in this work, future optimizations could employ a constrained or multi-objective, multiphysics
39 scheme that minimizes both the fuel temperature and the cycle length reduction in a trade-off study.

40 **2.2. Overview of generic algorithms employed in the present study**

41 GAs are a subset of evolutionary algorithms that are inspired by genetics and the Darwinian theory of
42 natural selection [17]. The primary operators that enable optimization with GAs are crossover and
43 mutation [17, 18]. *Crossover* is the creation of offspring by combining the genetic material of two parent
44 solutions, and *mutation* is the act of making random changes to the genetic material of a solution.
45 *Selection* is the process by which two parent solutions are chosen for crossover, typically with preference

1 given to solutions with higher fitness scores (i.e., the measure of how well each solution meets the
 2 optimization objective). An in-depth review of GAs—including the various methods for selection,
 3 crossover, and mutation—is given by Katoch et al. [19].

4 Termination of a GA typically occurs after a set number of generations or once the entire population has
 5 converged to a single solution. The population-averaged Hamming distance, which in the context of GAs
 6 is the number of genes that are different between two solutions, can also be used as the convergence
 7 criterion [20]. Because of mutation events, the convergence of all individuals within the population to
 8 exact copies of each other is unlikely, so the population-averaged Hamming distance was used as the
 9 convergence criterion for these analyses.

10 3. Methodology

11 3.1. Finite Element Model Description

12 All finite element modeling was performed using ANSYS Mechanical, Release 21.2 [21]. A simple UO₂
 13 fuel pellet model was developed with typical PWR geometry and linear heating rate (Table 1). The
 14 surface temperature of the pellet was set to 500°C, which is representative for a PWR fuel pellet with
 15 average linear heating. Coarse mesh and fine mesh schemes were used for modeling and are also
 16 summarized in Table 1 along with the reference geometry and boundary conditions. The two mesh
 17 schemes were used in varying capacities, as described in the following sections. All finite element
 18 modeling used internally maintained material property files for UO₂ and Mo; the temperature-dependent
 19 UO₂ properties are from the FRAPCON-3 fuel performance code for fresh fuel [22], and Mo properties
 20 are from the CINDAS, LLC, material property database [23]. The UO₂ phase was modeled as unirradiated
 21 fuel with 95% theoretical density.

22 **Table 1. Pellet model geometry, boundary conditions, and mesh schemes**

	Coarse mesh scheme	Fine mesh scheme
Pellet radius (mm)	4.1	4.1
Linear heating rate (kW/m)	18	18
Surface temperature (°C)	500	500
Pellet height (mm)	10	5
Nominal mesh element size (mm)	0.75	0.20
Number of elements	3,206	9,825
Symmetry method	Full symmetry	Octant symmetry (quarter symmetry azimuthally and half symmetry axially)

24 3.2. Methods for Mo Modeling

25 ANSYS parametric design language (APDL) scripts were developed to add Mo to the monolithic UO₂
 26 model. Two approaches were used for adding Mo to the base UO₂ pellet model. The Mo volume fraction
 27 was set to 10% for both methods because UO₂-Mo (10 vol % Mo) has been fabricated in several previous
 28 studies [8, 1, 9], so comparisons can be made between the simulated and fabricated fuels. The first
 29 method for developing the composite fuel was to overlay Mo line elements on the pellet model mesh, and
 30 the second method replaced entire 3D mesh elements of UO₂ with Mo. The inspiration for these two
 31 approaches traces back to the concepts used in previous UO₂-Mo studies, which typically focused on
 32 either composite microstructures or embedded heterogeneous Mo structures. The line-element approach

1 used here generated Mo configurations that resemble micro-networks, whereas the 3D element approach
2 enabled both micro-networks and structures. It was assumed that no heat was produced in the Mo phase in
3 either approach, and differential thermal expansion between the UO_2 and Mo phase was not considered.
4 The top and bottom of the pellet in both implementations was assumed adiabatic.

5 In the line-element approach, Mo was added to the pellet model based on a starting node, direction vector,
6 and total chain length. The APDL script added Mo line elements from the starting node, N_0 , to the nearest
7 node along the direction vector, N_1 . For the next line segment, N_1 became N_0 , and the chaining process
8 continued until the prescribed chain length was met, the pellet boundary was reached, or the total Mo
9 volume fraction constraint was met. In the algorithm's first iteration or during subsequent mutation
10 events, the prescribed chain length was randomly chosen between 0 and the length of a chain that would
11 take up 10% of the pellet volume. Each chain length was recorded as a gene and passed on to future
12 generations. Additional Mo line elements were added to the model in a similar fashion until the 10% Mo
13 volume fraction was reached.

14 ANSYS line elements represent 1D heat transfer connections between two nodes and therefore no heat
15 transfers through the radial surface of the line elements (i.e., from the wire centerline through the wire
16 radius). Radial heat transfer from the centerline of the wire to the UO_2 phase is negligible because of the
17 stark difference between UO_2 and Mo thermal conductivities. Heat can still be transferred radially out of
18 the pellet through the line elements if they are oriented in the radial direction, and heat generated in the
19 UO_2 phase can traverse azimuthally into the Mo line element. The primary limitation to this approach is
20 that heat transferring through the Mo line elements can only transfer between two nodes connected by a
21 Mo line element. In the 3D element approach, there are additional nodes in each Mo element for heat to
22 transfer to, which may distribute the heat in a more optimal fashion.

23 A line diameter of 0.5 mm was assigned to each line element to calculate the heat transfer area and the
24 total volume of Mo added to the pellet. This wire diameter was selected because it represents a typical
25 fabrication limit for precise AM techniques, such as laser powder bed fusion, that might be considered
26 when fabricating a Mo insert or composite fuel. Although the wire diameter affects the heat flux between
27 nodes, this parameter was not considered as a free variable to maintain a reasonable design exploration
28 space. Previous works on UO_2 -Mo pellet designs have indicated that smaller structures that uniformly
29 cover the pellet in the axial and azimuthal directions prevent hotspots and are more conducive to
30 maximizing heat transfer efficacy [12]. The Mo line elements do not displace any UO_2 in the model but
31 rather are overlaid on top of the UO_2 . Therefore, no adjustment to the power density in the UO_2 is
32 needed to produce the same amount of heat as in the monolithic UO_2 model. The coarse mesh scheme
33 detailed in Table 1 gave approximately the same results as the fine mesh in comparison tests and was used
34 for the line-element approach.

35 The implementation of the 3D element approach was like that of the line element approach. The UO_2
36 mesh elements were swapped with Mo based on a starting element E_0 , a direction vector, and a total chain
37 volume. The built-in techniques for spatial navigation in ANSYS are nodal based, so the nearest node to
38 E_0 along the direction vector was selected, and the element whose centroid was nearest to the selected
39 node E_1 was assigned Mo properties and became the next E_0 . As with the line-element method, each
40 elemental chain terminated when the prescribed chain volume (randomly selected between 0 and 10 vol
41 %), pellet boundary, or 10% Mo volume fraction were reached. A pellet model with quarter symmetry
42 azimuthally, half symmetry axially, and fine mesh scheme (Table 1) was used for the 3D element
43 approach to enable high-fidelity rendering of Mo structures while maintaining a reasonable optimization
44 search area, which is proportional to the number of mesh elements. Because entire UO_2 voxels were being
45 swapped with Mo, the power density in the UO_2 phase was enhanced by a factor of 1.1 to maintain the

1 same total power as the monolithic UO_2 model. The power distribution in the UO_2 phase in both the line
2 element and 3D element approaches was assumed to be uniform, although self-shielding in thermal
3 reactors would cause some radial power peaking in the pellet. Future analyses could apply neutronics
4 methods to determine the radial power profile in each pellet design.

5 The optimal designs produced by the GAs using both the line element and 3D element approach are
6 presented in Sections 4.2 and 4.3, respectively. Because of the random nature of how Mo is added to the
7 pellets in both approaches, it is possible for suboptimal structures to be added to the pellet. For example,
8 axially oriented structures are less conducive to heat transfer, although the displacement of UO_2 and
9 alteration of the power profile in the 3D element approach may assist in lowering fuel temperatures.
10 Large azimuthal gaps between Mo structures may also lead to heat accumulation and temperature peaks
11 in the UO_2 phase. The GAs attempt to eliminate these suboptimal structures via the fitness function and
12 crossover operation.

13 **3.3. Implementation of GA methods to UO_2 -Mo optimization**

14 Python scripts were developed to perform all GA-related functions, including calculating the fitness
15 function, parent selection, crossover, and mutation. The Python scripts generated APDL-readable input
16 files that contained the genes for each solution. The APDL macros loaded the pre-saved ANSYS
17 Workbench database files, which contained the base pellet model and mesh information, ensuring that the
18 same mesh (including the numeric identifier of each node and element within the mesh) was used for all
19 simulations. Then, the Python-generated input files containing the gene information for the entire
20 population were read into ANSYS, and several loops were executed to add Mo to the UO_2 base pellet
21 model, calculate the solution, and export the critical results for each solution to an output text file. The
22 Python script then read the output file produced by the ANSYS simulations and calculated the fitness
23 scores for each solution to begin the next generation of the GA.

24 In the context of the UO_2 -Mo GA, the solution genes were a vector rather than a single value. The genes
25 defined all the Mo chains in the solution, and each gene included a chain identification number, the
26 starting node or element, the direction vector (axial and azimuthal angles), and length or volume of each
27 chain. Because the volume of each chain could vary but the total Mo volume fraction was constrained to
28 10%, each solution could have a different number of genes. Several additional genes, referred to as the
29 *chaining fraction* and *branching fraction*, were a part of each chromosome in the line element approach
30 that described the overall solution. The chaining fraction is a probability that was defined as the number
31 of Mo chains that originated at the same node where a previous chain terminated, thus producing a longer
32 chain (but with the possibility of going in a different direction). The branching fraction was also a
33 probability that was defined as the number of Mo chains that originated somewhere along the length of a
34 previously defined chain, branching off in a different direction but maintaining a connected network.
35 These additional genes provided information on the connectedness of the optimal solution—whether it
36 was a continuous or a dispersed network of Mo—and were also used in probability tests that determined
37 the placement of new Mo chains. These genes were not included in the element approach, thereby
38 avoiding biasing the solution toward a widespread Mo network in contrast to solid structures.

39 A constant population size per generation of 50 was used for both GA approaches. Recommendations for
40 GA population sizes can vary greatly and are problem specific, but typically range from at least 20 up to
41 several hundred [24]. The arbitrary choice of 50 chromosomes per generation is considered sufficient for
42 this proof-of-concept analysis, but improvements may be realized by using larger populations or a
43 variable population size [25]. Premature convergence resulting from a population size on the lower end of
44 typical recommendations is counteracted in this work by using adaptive crossover and mutation rates and

1 by simulating many generations. The Python scripts that drove the GAs did not randomly select starting
 2 nodes/elements, direction vectors, or chain lengths. Rather, all random gene selections were made by the
 3 APDL script because the mesh information was contained in the ANSYS Workbench database file.
 4 During the GA initialization phase, each member of the population was assigned a single gene containing
 5 flags signaling that each parameter for placing the Mo chains should be selected randomly. The random
 6 selections were made in the APDL process after the mesh data were loaded, and a Mo chain was added to
 7 the model following the steps described in Section 3.2. The macro then added Mo chains to the model via
 8 random gene selections until 10 vol % Mo was achieved. In the line-element approach only, several
 9 probability tests based on the chaining and branching fractions were used to determine whether the new
 10 chain should extend an existing chain, branch off from an existing chain, or start a new chain altogether.
 11 These chaining and branching fractions were recorded as genes for each solution and therefore were
 12 passed along to future generations to determine the optimal connectedness of the Mo line-element
 13 network. Once it was determined whether to extend an existing chain, branch off from an existing chain,
 14 or start a new chain, N_0 was randomly selected from the subset of nodes that met the criteria.

15 Once the Mo was positioned, the ANSYS Workbench calculation was executed. The primary figure of
 16 merit was the maximum nodal temperature, which was recorded for all solutions in the population. After
 17 all 50 simulations in the population completed, the peak temperatures for each simulation were
 18 communicated back to the Python script driving the GA. The fitness score for each solution was
 19 determined using Eq. (2), which is effectively a measure of the relative peak temperature reduction
 20 compared with the monolithic UO_2 model:

$$f_i = \frac{T_{max,UO_2} - T_{max,UO_2-Mo_i}}{T_{max,UO_2}}, \quad (2)$$

21 where f_i is each fitness score, T_{max,UO_2} is the centerline temperature in the reference UO_2 model, and
 22 T_{max,UO_2-Mo_i} is the peak temperature of each UO_2 -Mo solution. The bulk thermal conductivity of each
 23 solution was calculated using Eq. (1) with $\Delta T = T_{max,UO_2-Mo_i} - 500^\circ\text{C}$ to facilitate comparisons to
 24 reported thermal conductivities in other works.

25 The roulette wheel method [26] with elitism [27] was used for parent selection in the GAs. Roulette wheel
 26 selection involves ordering the individuals from the current generation from highest to lowest fitness
 27 score, and the fitness scores are normalized so that they sum to 1. A random number between 0 and 1 is
 28 selected, and the individual for which the partial sums of normalized fitness scores surpass the random
 29 number is chosen as a parent [26]. The probability of selection in the roulette wheel method is therefore
 30 proportional to each fitness score. In elitism, the single best solution from each generation is copied into
 31 the next generation to ensure the peak fitness score never decreases. Selection is performed with
 32 replacement in the roulette wheel method, so an individual could be selected as a parent more than once.

33 In addition to the maximum fuel temperature, the temperature gradient per unit length ($\Delta T/L$) for each
 34 Mo chain was also calculated during the ANSYS simulations in the line-element approach only. These
 35 values were exported to the Python driver script and used for a unique crossover method implemented in
 36 this analysis. This parameter was considered a measure of heat transfer efficiency because it is
 37 proportional to heat flux. The thermal conductivity was the constant of proportionality, and a “best chain”
 38 crossover method was developed that passed on the chains from both parents that had the largest
 39 temperature decrease per unit length. This method was used to accelerate the GA because chains that
 40 produced only a small linear temperature decrease were not conducive to the optimization objective. No
 41 analogous method was developed for the 3D element GA because the possibility that structures could be

1 created near the centerline of the pellet did not necessarily enhance heat transfer but instead prevented
2 hotspots or pushed the peak fuel temperature away from the centerline. For this reason, single-point
3 crossover was used in the element-based GA.

4 A two-tier mutation approach was taken because each gene is a vector of four values for these specific
5 GAs. The *allele mutation probability* (referencing the name given to the specific value that a gene takes in
6 common GA terminology) determined whether a single value within each gene vector would mutate, and
7 the *gene mutation probability* determined whether the entire gene vector was mutated. The gene mutation
8 probability was arbitrarily set to one-fifth of the allele mutation probability in both GAs because mutation
9 rates typically are relatively small [28].

10 Adaptive crossover and mutation probabilities were implemented in the GAs to prevent premature
11 convergence on a local optimum (rather than the global optimum) using the methods described by
12 Srinivas and Patnaik [28]. In the following equations, f_{max} is the highest fitness score from a population,
13 \bar{f} is the population average fitness score, f_i is each individual's fitness score, and f' is the greater of the
14 two fitness scores of parents selected for crossover. The crossover probability, p_c , and allele mutation
15 probability, p_m , are then given by Eqs. (3) and (4):

$$p_c = \begin{cases} (f_{max} - f') / (f_{max} - \bar{f}) & , f' > \bar{f} \\ 1 & , f' \leq \bar{f} \end{cases} \quad (3)$$

$$p_m = \begin{cases} 0.5(f_{max} - f_i) / (f_{max} - \bar{f}) & , f_i > \bar{f} \\ 0.5 & , f_i \leq \bar{f} \end{cases} \quad (4)$$

16 Based on the equations, the crossover rate can vary from 0–1.0, and the allele mutation rate can vary from
17 0–0.5. The gene mutation rate therefore varies from 0–0.1, and the maximum values of the allele and gene
18 mutation rates are higher than those typically used in GAs with static mutation rates (≤ 0.05 is common).
19 The adaptive methods developed by Srinivas and Patnaik [28] are considered widely applicable due to the
20 large range of possible values for p_c and p_m , which are calculated for each individual solution, and avoid
21 the pitfalls of using constant values that are often arbitrary and problem specific. This approach enables
22 design exploration and exploitation simultaneously because solutions with low fitness scores have a much
23 higher chance of mutating and solutions with high fitness scores are retained and crossover with each
24 other to exploit local optima.

25 A notable feature of this adaptive scheme is that the crossover and mutation probabilities vary for
26 each generation and for each pair of parents (for crossover) or individual (for mutation). The bottom half
27 of solutions—if they are selected to be a parent—are assigned higher crossover and mutation
28 probabilities, and the best solution does not crossover or mutate at all. Because the higher fitness function
29 solutions are preferably selected for recombination, mutation and crossover rates typically reach high
30 values only when population diversity is low and most solutions have a very similar fitness score.
31 Combining the adaptive crossover and mutation probabilities with the roulette wheel selection method
32 allowed for the possibility that the best solution could be copied into the new generation multiple times. A
33 caveat to the dynamic crossover and mutation probability approach was added so that the first occurrence
34 of the best solution being chosen as a parent was copied “as is” into the new generation (as part of the
35 elitism strategy). Additional occurrences were assigned a mutation probability of 1% to explore
36 incremental changes to the best design. Other approaches for preventing convergence on a local optimum,
37 such as maintaining a constant fraction of random solutions or initiating the GA with a larger population

1 to spread the exploration space, were not considered for this proof-of-concept analysis but could be
2 considered for future applications.

3 Owing to the nature of the optimization problem, each solution has a variable number of genes because
4 each gene is a variable-length Mo chain and the total Mo volume fraction is constrained to 10%. A result
5 of this feature and the crossover and mutation operations is that many solutions will be generated that do
6 not meet the 10 vol % Mo constraint. To prevent this issue, the APDL script tracked the total volume of
7 Mo in all solutions. If a solution reached 10 vol % Mo but still had additional genes to implement, then
8 those genes were truncated. Additional Mo chains were stochastically added to solutions that did not
9 reach 10 vol % Mo.

10 A modified Hamming metric was used in conjunction with a non-improvement counter to determine
11 when to terminate the algorithm. Because the mesh numbering scheme was identical for every solution,
12 the nodes or elements that contained Mo could be compared between a pair of solutions to determine
13 what fraction of Mo had been positioned in the same location. This comparison was made between all
14 members of the population in each generation, and a population-averaged gene similarity factor was
15 calculated. The line-element GA was terminated once the average fraction of shared genes exceeded 95%
16 and 150 generations passed without an improvement to the best design. For the element-based GA, the
17 algorithm was allowed to execute 250 generations without improving once the population shared more
18 than 95% of their genes. A detailed summary of the GAs, including aspects unique to the current
19 optimization problem, is presented in Figure 1.

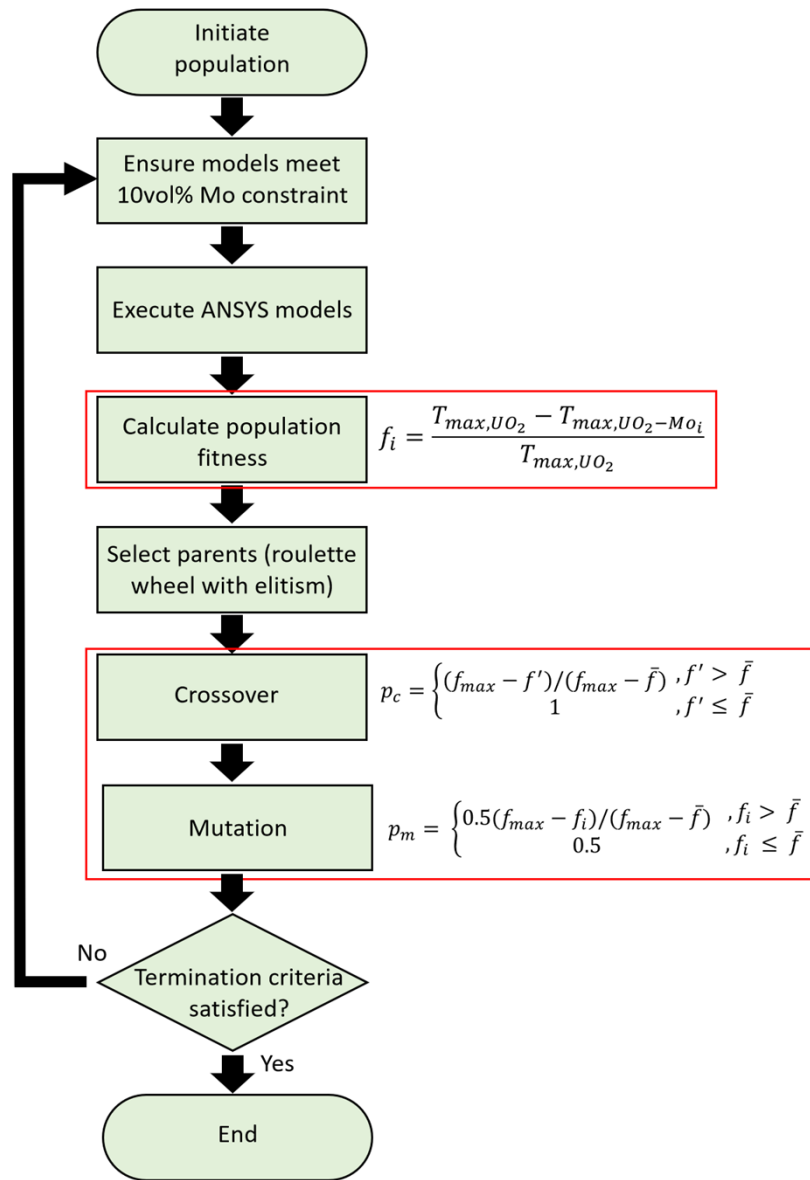
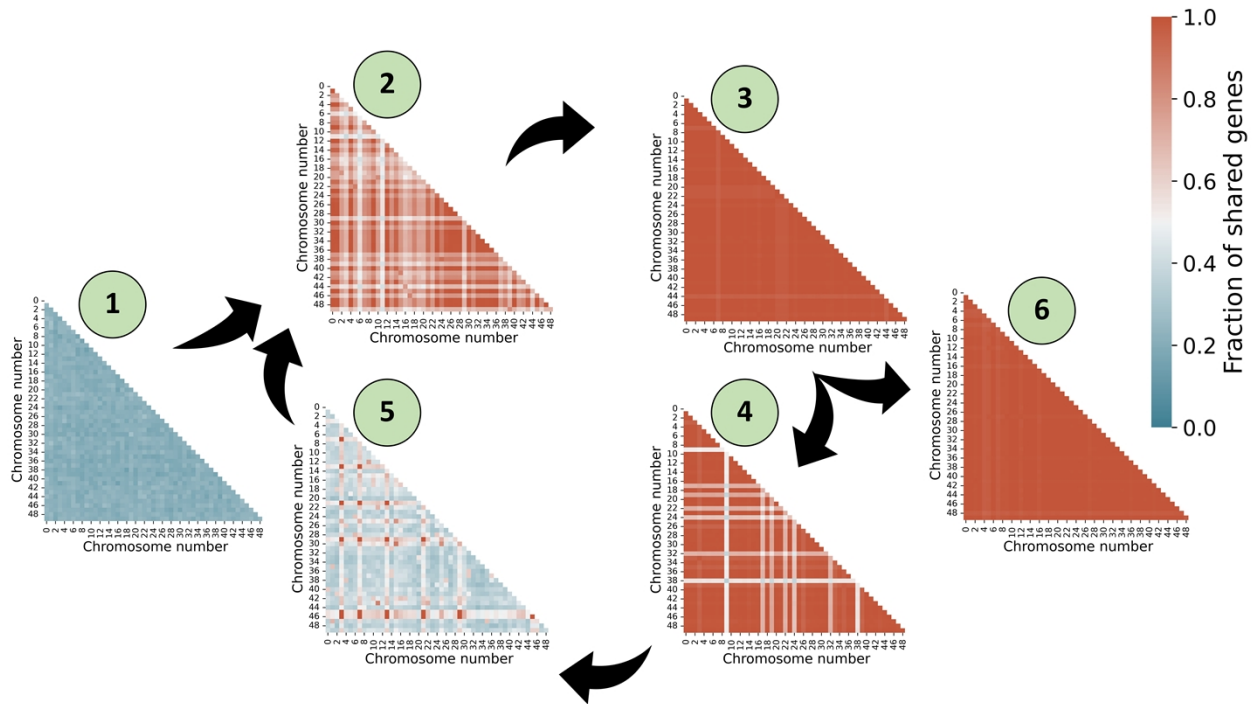


Figure 1. GA flowchart.

Figure 2 illustrates how the population convergence evolved during algorithm execution using triangular matrices that indicate the fraction of shared genes between each member of the population. The x - and y -axes of each subplot are zero-indexed identification numbers for each member of the population (with a population size of 50) so that each solution can be compared to every other solution. Descriptions of each numerical callout in the figure are as follows:

1. Random initialization (generation 1). Population diversity is very high.
2. The population starts converging on a local optimum. Because the roulette wheel parent selection method was used, the solutions chosen for reproduction typically have higher than average fitness

- 1 scores, and the crossover and mutation probabilities are relatively low. The algorithm focuses on
 2 exploiting a local optimum.
- 3 3. The low crossover and mutation rates cause the population to converge on a single solution, and the
 4 range of fitness scores is small because most members of the population are near or exact copies of
 5 each other. Consequently, even the parents chosen for reproduction have a significant chance of
 6 having a fitness score that is less than or equal to the population average, and crossover and mutation
 7 probabilities become very high. This stage is considered a local optimum, if not the global optimum.
- 8 4. The high rates of crossover and mutation yield a new optimal solution. The crossover and mutation
 9 probabilities remain high because only one or a few solutions have the new high fitness score and
 10 most fitness scores are at or below average.
- 11 5. If the new optimal solution has moved into a new local optima, then the high crossover and mutation
 12 rates may drive a high degree of population diversity where only a few solutions are similar to each
 13 other. The population may not always reach the level of diversity illustrated in the figure at this stage.
- 14 6. The GA will iterate steps 2–5 until high mutation and crossover rates can no longer drive an
 15 improvement. At this point, the GA terminates and the population is assumed to have converged on
 16 the global optimum.

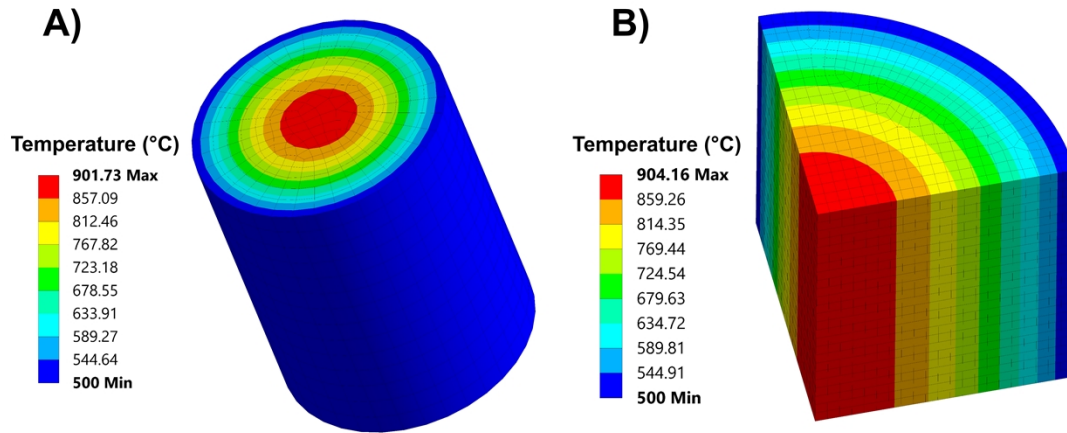


17
 18 **Figure 2. Illustration of population diversity while searching for the global optimum.** The x- and y-axes of each
 19 subplot are zero-indexed identification numbers for each member of the population (with population size of 50).
 20 Each subplot was pulled from various points throughout the optimization execution to illustrate the cyclic nature of
 21 population diversity.

1 4. Results

2 4.1. Reference Model Mesh and Results

3 The two mesh schemes and associated temperature distributions in the coarse- and fine-mesh UO_2 models
4 are shown in Figure 3. The centerline temperatures predicted using the coarse- and fine-mesh schemes
5 were 901.7°C and 904.2°C , respectively. A third solution was generated using an even more refined mesh
6 scheme (74,250 total elements compared to 3,206 and 9,825 for the coarse and fine mesh schemes,
7 respectively, used for the GAs) that still predicted a centerline temperature of 904.2°C , indicating that the
8 mesh used for the 3D-element-based GA was sufficiently refined. The 2.5°C difference between the two
9 mesh schemes is likely due to the absence of nodes located in the precise center of the pellet in the coarse
10 mesh. For the purposes of this analysis, the line-element-based approach with coarse meshing can be
11 considered illustrative of GA optimization applied to nuclear fuel design. As the subsequent sections
12 show, the element-based approach resulted in a better performing fuel design.

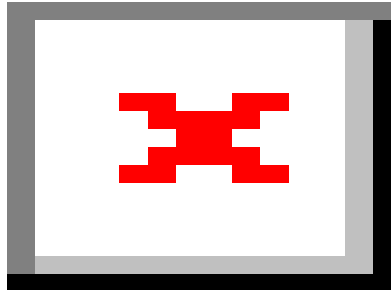


13
14 **Figure 3. Reference temperature distributions in monolithic UO_2 using the (A) coarse-mesh scheme and (B)**
15 **fine-mesh scheme.**

16 4.2. Line-Element GA Results

17 Figure 4 shows plots of the bulk thermal conductivity (Eq. [1]) and peak fuel temperature of the highest-
18 fitness solution as a function of the number of simulated generations for the line-element-based GA. The
19 highest performing solution from the initial generation had a maximum temperature of 755.5°C , which is
20 a 12.4% decrease from the reference peak temperature for this set of boundary conditions when
21 converting to the kelvin scale (all relative temperature comparisons in this paper were performed by first
22 converting the temperatures to kelvin). Initially, the maximum temperature decreased rapidly with each
23 passing generation, but the incremental improvements to the design slowed as the algorithm progressed.
24 By the 10th generation, the maximum temperature had decreased to 674.2°C . By the 100th generation, the
25 maximum temperature had decreased to 660.8°C . The rapid design improvement that occurs early in the
26 GA was likely caused by using the “best chain” crossover method, which preferentially passed on Mo line
27 elements with large temperature gradients per unit length. The algorithm simulated 4,004 generations
28 (200,200 total model runs with 50 simulations performed per generation) before the termination criteria
29 were met, and the final maximum temperature of the highest performing design was 635.3°C . This result
30 equates to a 22.7% reduction in the maximum fuel temperature compared with the monolithic UO_2 pellet
31 and a decrease in the ΔT across the fuel pellet from 401.7°C in the coarse mesh reference model to

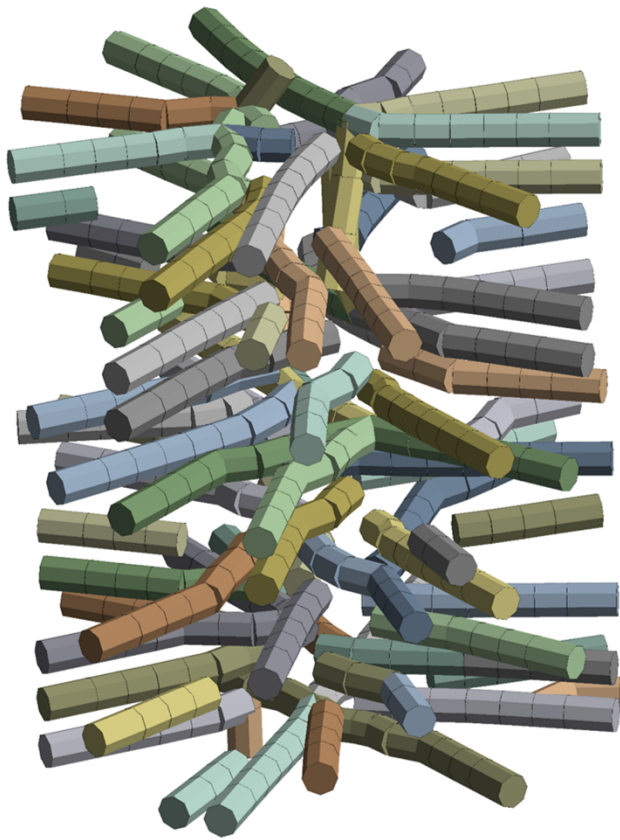
1 135.3°C in the optimized pellet. The associated bulk thermal conductivity was 10.6 W/m·K, or roughly
2 three times the bulk thermal conductivity of 3.5 W/m·K for the UO₂ model.



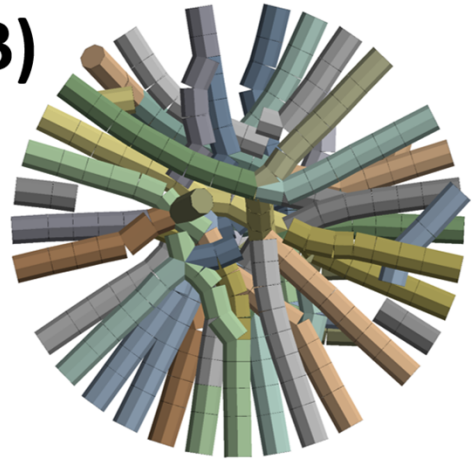
3
4 **Figure 4. Evolution of highest fitness solution thermal conductivity and maximum fuel temperature as a**
5 **function of simulated generations.**

6 Several views of the optimized line-element solution are shown in Figure 5. Prominent features of the
7 design are that the Mo line elements are predominantly oriented in the radial direction, the line elements
8 are arranged in layers with equal axial spacing, and the largest spacing between line elements appears to
9 occur in the azimuthal direction. To further illustrate the characteristics of the optimal design, Figure 6
10 presents the Mo vol % in 8 equal thickness radial regions and 10 equal thickness axial regions. The
11 number of binning regions used in the radial direction was limited by the coarse-mesh scheme. Figure 6A
12 shows that the Mo concentration peaks at a relative radius of about 0.2 and then steadily decreases as the
13 radius increases. In the axial direction, the Mo concentration is roughly symmetric across the pellet height
14 and exhibits alternating high/low concentrations. The peak Mo volume percentage occurs near the axial
15 midplane.

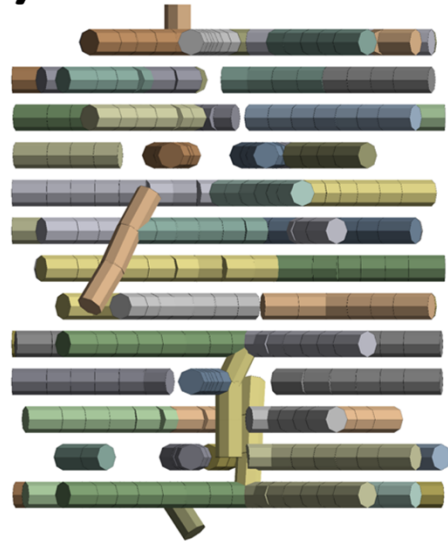
(A)



(B)

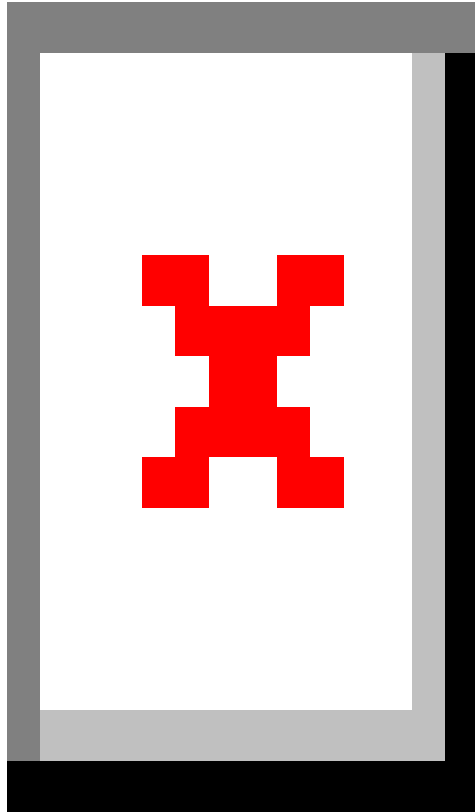


(C)



1
2
3

Figure 5. Depiction of optimized Mo geometry from the line-element-based approach in (A) isometric, (B) top, and (C) side views. Line element diameters are to scale.



1
2
3

Figure 6. Mo vol % in equal-thickness (A) radial regions and (B) axial regions in the line-element-based solution.

1 4.3. Element Based GA Results

2 The element-based GA executed 5,200 generations, which coincided with 250 generations without a
3 design improvement and a population-averaged gene similarity factor greater than 95%. The peak fuel
4 temperature and thermal conductivity evolved similarly as the line element GA values shown in Figure 4
5 but reduced the peak fuel temperature to 626.2°C, equating to a bulk thermal conductivity of 11.3
6 W/m·K, a ΔT across the fuel pellet of 126.2°C (compared to 404.2°C in the reference fine mesh model),
7 and a 23.6% reduction in peak fuel temperature from the UO₂ reference model. Figure 7 shows several
8 views of the Mo configuration in the optimized pellet.

9 The Mo phase shown in Figure 7 takes three distinct forms, including dispersed Mo consisting of one or a
10 few elements, generally linear chains of Mo elements oriented radially, and a large structure with Mo
11 elements/chains branching from it. To better illustrate the Mo geometry, Figure 8 shows a visual
12 expansion of the symmetric pellet model unfolded into a full pellet and distinguishes between the three
13 general types of structures. An STL file of the pellet mesh is included as supplementary material to this
14 article. The dispersed Mo form (Figure 8B) is most heavily concentrated near the pellet centerline;
15 therefore, very little heat transfers through most of the elements in this category. Rather, these elements
16 alter the distribution of heat generation, and the Mo concentration at the centerline is high enough to
17 move the peak fuel temperature radially outward by 0.6 mm. The roughly linear chains of Mo elements
18 (Figure 8C) originate in the mid-to-outer radial region of the pellet and extend to the pellet outer surface
19 (i.e., they appear in regions of relatively high heat flux and lower temperatures).

20 The third structure (Figure 8D) is continuous and roughly resembles stacked fins that fan and branch
21 outward near the pellet outer radius. This large structure extends the entire pellet radius and height and
22 accounts for 87.7% of the total Mo in the pellet. The fin-like structures have a roughly 90° azimuthal
23 separation and contain many voids in the axial direction. This structure is likely necessary to minimize
24 heat transfer through UO₂ in the radial direction. The Mo chains branch off from the structure in several
25 locations, such as those seen on the left and right side of the top-down view of the continuous Mo
26 structure in Figure 8D. The top and bottom of the continuous Mo structure (from a top-down view) does
27 not have these finger-like connected branches, but the Mo chains (Figure 8C) fill in the voids between the
28 continuous Mo structure so heat transfers through a minimal amount of UO₂. The pellet mesh also has
29 some influence on the resulting structures. The chain structures that are not connected to the larger
30 structure are azimuthally located among the four major fins, and the dispersed Mo phase fills in some of
31 the voids near the pellet centerline in the larger structure.

32 Figure 9 shows the temperature distribution in the optimized pellet model and the heat flux vectors
33 through a slice of the fuel pellet. The lengths of the heat flux vectors in Figure 9B are proportional to the
34 magnitude and indicate that the heat flux through the Mo phase increases with increasing radius while the
35 heat flux through the UO₂ phase remains very small (compared with the heat flux in the Mo regions)
36 throughout.

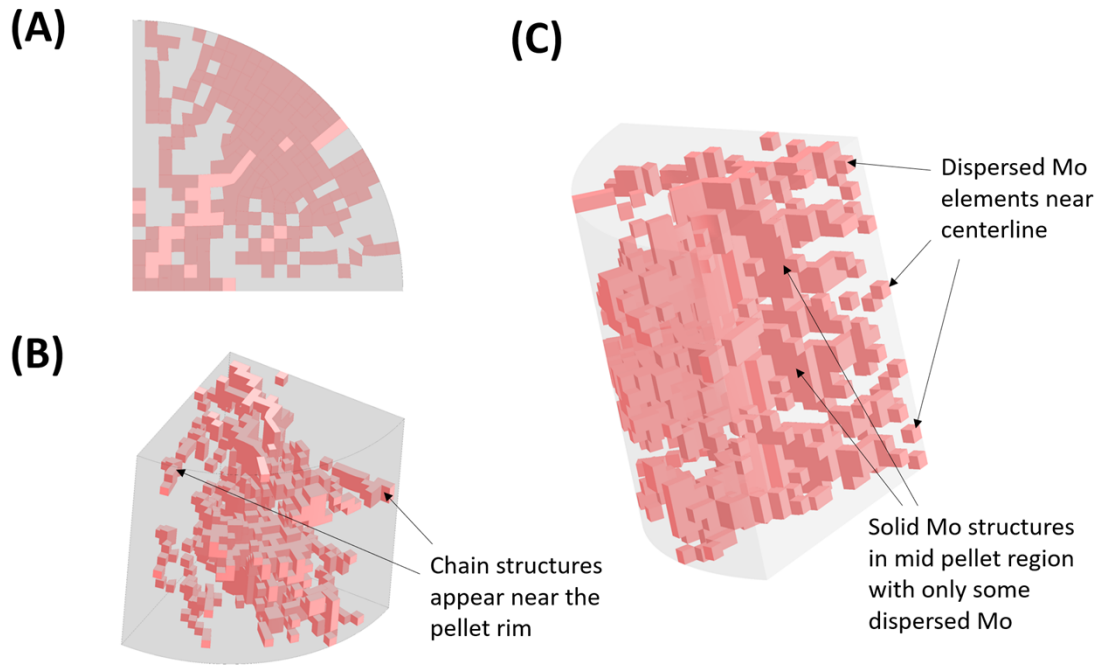


Figure 7. Depiction of optimized pellet from element-based approach.

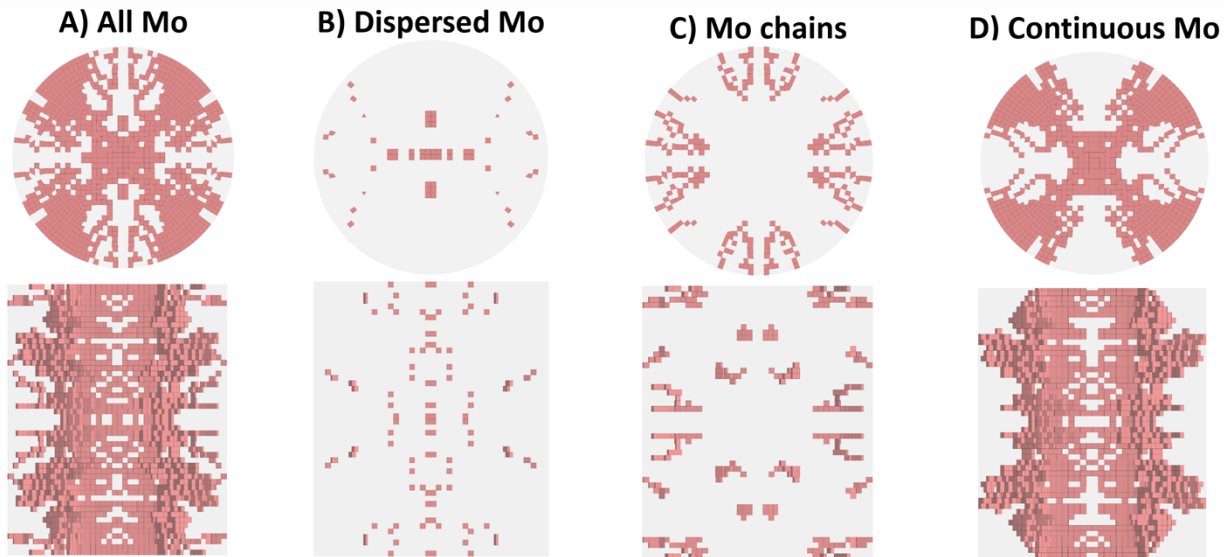
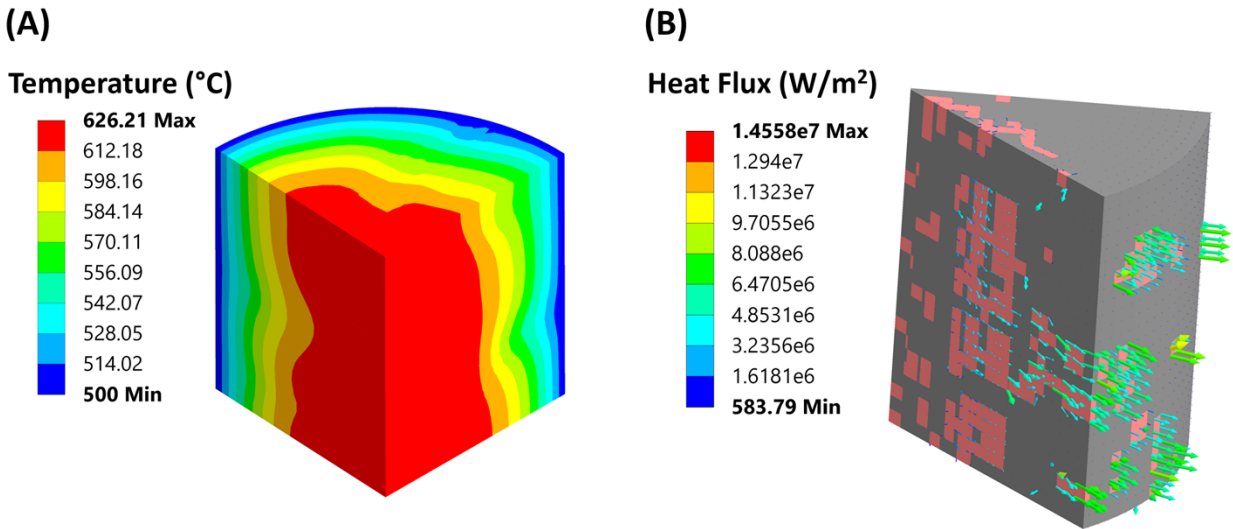


Figure 8. Visual expansion of optimized UO_2 -Mo pellet and depiction of various Mo structures.

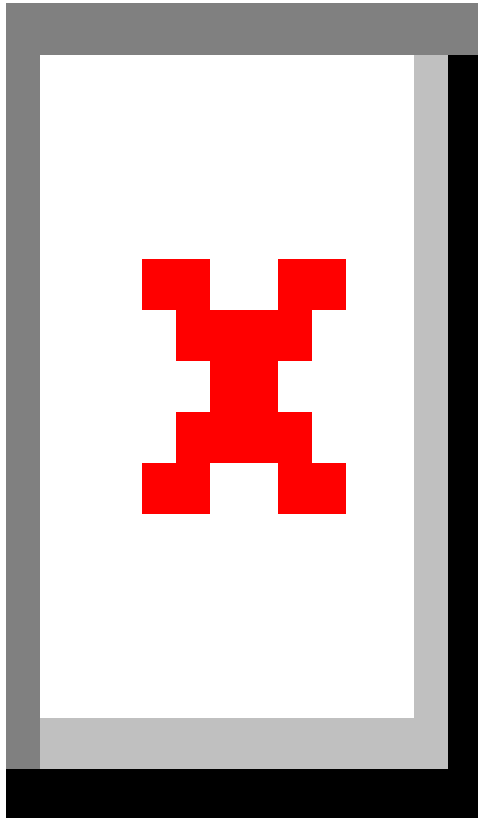
1



2

3 **Figure 9. (A) Temperature distribution in optimized pellet. (B) Heat flux vectors through a slice of the**
4 **optimized pellet.**

5 Figure 10 characterizes the distribution of Mo in the optimized pellet. As before, the figure shows the Mo
6 vol % in equal-thickness radial and axial regions. Each bin in the axial direction represents a one-element-
7 thick layer, and the Mo concentration in each layer is exactly 10 vol %. The concentration in the radial
8 direction varies between ~8 and 12 vol % but is relatively uniform across the pellet radius.



1
2
3

Figure 10. Mo vol % in equal-thickness (A) radial regions and (B) axial regions in the 3D element-based solution.

1

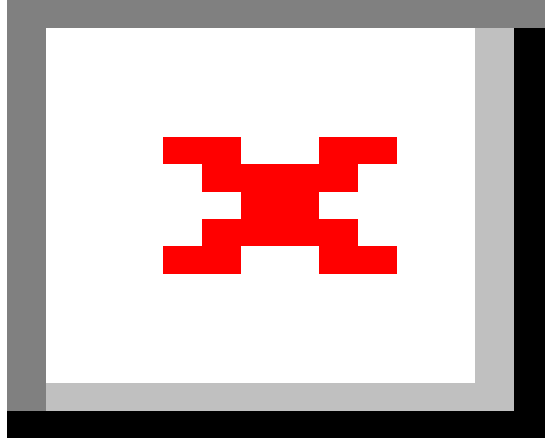
2 To obtain a temperature-dependent correlation for the optimized pellet's thermal conductivity, additional
3 ANSYS cases were executed in which the relative pellet power was varied from 10% to 225% of the
4 nominal value, and the pellet outer surface temperature was varied from 0°C to 1,000°C. The resulting
5 thermal conductivity correlation was then compared with the thermal conductivity of several fabricated
6 UO₂-Mo (10 vol % Mo) designs—including from Buckley et al. [1], Finkeldei et al. [8], and Kim et al.
7 [9]—and to commonly used methods for approximating composite material properties. These
8 approximations include the volume-weighted rule of mixtures (ROM), the inverse ROM (iROM), and the
9 Maxwell equation for estimating bulk properties of particles dispersed in a matrix [29] and are given in
10 Eqs. (5)–(7), respectively.

$$k_c = \sum_i^n V_i k_i, \quad (5)$$

$$\frac{1}{k_c} = \sum_i^n \frac{V_i}{k_i}, \quad (6)$$

$$k_c = k_m \frac{k_p + 2k_m + 2V_p(k_p - k_m)}{k_p + 2k_m - V_p(k_p - k_m)}, \quad (7)$$

11 where k represents thermal conductivity, V represents the phase volume fraction, subscript c denotes the
12 composite material, i denotes each phase in the composite, m denotes the matrix material, p denotes the
13 dispersed particle phase, and n is the total number of phases in the composite. The thermal conductivity
14 correlations for UO₂ and Mo used in the ROM, iROM, and Maxwell equations are the same as those used
15 in the ANSYS model [22, 23]. Figure 11 displays plots of the thermal conductivity correlations and
16 shows that the pellet design produced by the GA exhibited a greater thermal conductivity than any of the
17 fabricated fuels. The only thermal conductivity correlation that predicted a greater thermal conductivity
18 than the GA design was the ROM approximation. However, a ROM approximation overestimates
19 attainable values for thermal conductivity of ceramics and refractory composite materials, particularly for
20 the case in which the thermal conductivity of the constituent phases differs significantly, as in the present
21 investigation [30].



1
2 **Figure 11. Comparison of UO_2 , Mo, and UO_2 -Mo (10 vol% Mo) thermal conductivity correlations [1, 8, 9, 29,**
3 **23, 22].**

4 **5. Discussion**

5 **5.1. GA Performance and Considerations**

6 Based on the thermal conductivity comparisons shown in Figure 11, the element-based GA developed a
7 UO_2 -Mo fuel pellet design that effectively minimized the fuel temperature. The optimized design features
8 a mixture of dispersed, continuous network, and solid-structure Mo configurations in a way that is not
9 necessarily obvious for minimizing the fuel temperature. However, the prevalence of radially oriented
10 features in both GA designs makes intuitive sense given that heat transfer occurs predominantly in the
11 radial direction in narrow cylinders. Enabling entire 3D UO_2 elements to be exchanged for Mo was key to
12 the higher performance of the second GA because the Mo phase in the optimized design enhanced heat
13 transfer efficacy and prevented hotspots by dispersing regularly near the centerline. Regular spacing of
14 dispersed Mo elements displaces UO_2 in the highest energy density region with low cost to the total Mo
15 volume fraction. Little heat is transferred across these elements, but their inclusion alters the distribution
16 of heat generated in the pellet and shifts the peak fuel temperature away from the centerline. The power
17 distribution would be further altered in a thermal reactor due to self-shielding in the pellet, which may
18 impact the location of the maximum fuel temperature. The line-element approach was solely focused on
19 enhancing heat removal, likely explaining the different Mo distributions between the two designs (Figure
20 6 and Figure 10). Because the Mo line elements were overlaid on the pellet mesh and did not displace
21 any UO_2 , the heat generation profile in the pellet is the same as in a monolithic UO_2 pellet.

1 Other features critical to high GA performance were the adaptive crossover and mutation probabilities.
2 Early iterations of the GAs used static probabilities and succumbed to premature convergence on
3 suboptimal solutions with thermal conductivities similar or lower than those found in the literature for
4 fabricated fuels. Dynamic crossover and mutation probabilities maintained population diversity and
5 facilitated incremental design improvements.

6 The GA approach demonstrated in this work could be leveraged for future fuel optimization activities that
7 aim to optimize some other aspect of fuel or reactor performance. The algorithms could also benefit from
8 additional development for multiobjective or constrained optimization studies to balance the effect of
9 multiphysics phenomena. For example, this work focused solely on heat transfer performance but
10 assumed perfect contact between the UO_2 and Mo phases and a uniform heat distribution in the UO_2
11 phase. Incorporating thermal expansion, stress calculations, and a power distribution informed by
12 neutronic self-shielding calculations may inform the mechanical stability of the fuel design (although the
13 significant temperature reduction should mitigate separation of the two phases owing to differential
14 expansion). A multiphysics strategy that accounted for the impact on reactor cycle length and radial
15 peaking in the pellet could investigate the trade-offs between Mo and other high-melting-point materials
16 with lesser neutronic penalties (e.g., Nb). The GA optimization methods could also be coupled with
17 sensitivity analysis to more robustly identify high importance regions in the pellet and to further optimize
18 the Mo orientation. Thermal contact resistance between the two phases and fuel cracking were not
19 considered in this work and may reduce the predicted performance. A more encompassing approach could
20 consider the thermal, mechanical, and neutronic performance of a UO_2 -Mo design and incorporate
21 computer aided design software to assist with fabrication.

22 Another important consideration for future analyses that intend to optimize a fuel design using finite
23 element models and GAs is the mesh scheme. The finite element mesh bounds the total design search
24 space, and ill-conceived meshes may prevent the global optimum solution from being found. However,
25 extremely fine mesh schemes drastically increase the algorithm runtime by increasing both the search
26 space and the time to execute each individual solution. In this work, this consideration was addressed by
27 opting for a finer mesh and quarter symmetry in the 3D element approach.

28 **5.2. Fuel Fabricability**

29 The present study identified UO_2 -Mo composite architectures that significantly outperform conventional
30 composites of equivalent phase content in terms of thermal properties and thermal performance. The
31 optimized structures are predicted to reduce the maximum UO_2 fuel temperature by over 23%. This
32 reduction in operating temperature increases margin to melt and improves accident behavior by reducing
33 stored energy in the fuel. Improvements in other key fuel performance metrics (e.g., swelling, fission gas
34 release) generally accompany reduced homologous fuel temperature, as well. Numerous other activities
35 are needed to fully assess the performance of such a fuel form, but foremost in consideration is
36 fabricability.

37 Fabrication of the optimized fuel pellets designed in this work would require precise placement of the Mo
38 phase in the UO_2 phase. All literature examples of fabricating UO_2 -Mo fuels involve mixing UO_2 and Mo
39 particle feedstock followed by pressing and sintering the pellet. This process offers no control over the
40 placement of the Mo phase. Coupling AM of Mo inserts with UO_2 fabrication to achieve high thermal
41 conductivity engineered structures with the goal of improving heat transfer has been proposed [31], but
42 open literature examples of these systems and the attained properties do not exist. Other computational
43 studies of UO_2 -Mo fuel systems have assumed that either the UO_2 and Mo are separate and could be

1 stacked alternately in a fuel rod [13], or the Mo phase is a single standalone structure that the UO₂ could
2 be pressed and sintered around [12].

3 The GA-produced fuel pellet design could not be fabricated using traditional methods. Conventional
4 pellet fabrication methods can accommodate limited radial heterogeneities if axial continuity is retained.
5 Examples of such pellet architectures are annular pellets, duplex pellets, or pellets containing a central
6 inert rod [10]. AM methods are likely the only avenue for producing a fuel pellet approaching the
7 complexity identified in the present work. Even then, the methods capable of control on submillimeter-
8 scale Mo inclusions are yet to be developed [10].

9 Two strategies can be considered when developing a fabrication technique using AM to manufacture the
10 GA-optimized UO₂-Mo fuel system. The first approach is to use a metal AM process, such as selective
11 laser melting (SLM), to fabricate a Mo insert that could be incorporated into a die or mold with UO₂ for
12 traditional processing routes [31]. This process would demand a continuous Mo network for printing and
13 may have further geometrical constraints owing to the requirement of supports for overhangs at angles
14 less than approximately 45°. Additional Mo network modifications may need to be considered to
15 accommodate the resolution of the SLM process. SLM's feature resolution is defined by the laser spot
16 size in the x -, y -, or r -axes, which is approximately 100 μm for most commercially available systems [32].
17 The z -axis resolution is determined by layer thickness: a thickness of 30 μm can print dense Mo [33]. The
18 insert's mechanical strength must also be considered to allow for survival during pressing or molding of
19 the composite pellet. This strategy is likely viable at the laboratory scale with development, but scalability
20 would be a challenge.

21 A second manufacturing approach is to employ a multiple-material AM (MMAM) method capable of
22 printing ceramic/metal composite structures. Such processes are much less developed than the previously
23 discussed method but have the potential to be more effective. These processes would not constrain the Mo
24 to a continuous network. The most mature MMAM method that could be used is direct ink writing
25 (DIW), which is a slurry-based extrusion process. DIW allows for multiple slurries to be printed
26 simultaneously; one slurry could contain UO₂ and the other Mo to fabricate composites with full spatial
27 freedom of each material [34]. The geometric resolution of DIW is defined by the inner diameter of the
28 extrusion nozzle in the x -, y -, or r -axes, where diameters as low as 600 μm have been tested [35]. Like
29 SLM, z -axis resolution is defined by layer thickness; however, layer thicknesses around 1 mm are needed
30 for DIW. In addition to DIW, several other more complex MMAM processes could be screened for
31 manufacturing the optimized UO₂-Mo fuel system [36].

32 Developing and maturing new manufacturing methods for composite architectures such as those
33 evaluated here may provide additional fabrication options. If a specific AM method is identified for
34 further evaluation, then its constraints and limitations could be included in an optimization approach like
35 that presented herein. It may be possible to incorporate a fabricability parameter into the optimization
36 routines that imposes requirements of the specific manufacturing method employed. For example, Mo
37 elements could be of a minimum thickness or an extent of continuity could be required with the remainder
38 of the structure to be permissible. This approach could be extended to multiple AM methods (each
39 imposing unique fabricability constraints) to assess the achievable fuel thermal performance against
40 manufacturing economics.

41 **6. Conclusions**

42 In this work, two GA approaches were used to optimize a composite UO₂-Mo (10 vol % Mo) nuclear fuel
43 pellet in ANSYS finite element software. The GA, which overlaid Mo line elements over a UO₂ mesh in

1 one approach and exchanged 3D UO₂ elements for Mo in another, effectively produced composite fuel
2 designs with peak fuel temperatures that were approximately 23% lower than the reference UO₂ model
3 for the boundary conditions used, corresponding to a ΔT of 126°C–135°C across typical PWR fuel pellets
4 with representative power density. Radial power peaking in the fission power distribution in a thermal
5 reactor could have some effect on this observed temperature reduction. Compared with literature data of
6 fabricated UO₂-Mo fuels, the optimized fuels exhibited much higher bulk thermal conductivities. The
7 predicted thermal conductivities were also greater than the commonly used iROM and Maxwell equations
8 used for estimating composite fuel properties.

9 The dynamic adjustment of crossover and mutation probabilities were crucial aspects of the GA that
10 enabled the algorithm to escape premature convergence on local optima. Future developments in
11 composite fuel optimization could investigate multiphysics phenomena and mesh optimization to avoid
12 influencing the algorithm toward suboptimal designs. The highest performing design produced by the GA
13 involved a mixture of dispersed Mo elements at the centerline, a combination of solid structures and
14 continuous Mo networks in the mid-pellet region, and a high degree of network branching in the high-
15 heat-flux region near the pellet rim. Fabricating this complex design would require advanced AM
16 techniques.

17 ACKNOWLEDGMENTS

18 This work was initially funded by the Transformational Challenge Reactor program of the US Department
19 of Energy, Office of Nuclear Energy. Additional funding was provided by the National Nuclear Security
20 Administration, Office of Defense Nuclear Nonproliferation Research and Development.

21 22 7. Bibliography

- 23
- [1] J. Buckley, J. D. Turner and T. J. Abram, "Uranium dioxide - Molybdenum composite fuel pellets with enhanced thermal conductivity manufactured via spark plasma sintering," *Journal of Nuclear Materials*, pp. 360-368, 2019.
 - [2] K. A. Terrani, D. Wang, L. J. Ott and R. O. Montgomery, "The effect of fuel thermal conductivity on the behavior of LWR cores during loss-of-coolant accidents," *Journal of Nuclear Materials*, vol. 448, no. 1-3, pp. 512-519, 2014.
 - [3] R. Liu, W. Zhou, P. Shen, A. Prudil and P. K. Chan, "Fully coupled multiphysics modeling of enhanced thermal conductivity UO₂-BeO fuel performance in a light water reactor," *Nuclear Engineering and Design*, vol. 295, pp. 511-523, 2015.
 - [4] M. J. Notley and I. J. Hastings, "A microstructure-dependent model for fission product gas release and swelling in UO₂ fuel," *Nuclear Engineering and Design*, vol. 56, pp. 163-175, 1980.
 - [5] N. Capps, C. Jensen, F. Cappia, J. Harp, K. Terrani, N. Woolstenhulme and D. Wachs, "A critical review of high burnup fuel fragmentation, relocation, and dispersal under loss-of-coolant accident conditions," *Journal of Nuclear Materials*, vol. 546, p. 152750, 2021.

- [6] K. S. Kang, "Power uprates in nuclear power plants: International experiences and approaches for implementation," *Nuclear Engineering and Technology*, vol. 40, no. 4, pp. 255-268, 2008.
- [7] P. Hejzlar and M. S. Kazimi, "Annular fuel for high-power-density pressurized water reactors: Motivation and overview," *Nuclear Technology*, vol. 160, no. 1, pp. 2-15, 2007.
- [8] S. C. Finkeldei, J. O. Kiggans, R. D. Hunt, A. T. Nelson and K. A. Terrani, "Fabrication of UO₂-Mo composite fuel with enhanced thermal conductivity from sol-gel feedstock," *Journal of Nuclear Materials*, vol. 520, pp. 56-64, 2019.
- [9] D.-J. Kim, Y. W. Rhee, J. H. Kim, K. S. Kim, J. S. Oh, J. H. Yang, Y.-H. Koo and K.-W. Song, "Fabrication of micro-cell UO₂-Mo pellet with enhanced thermal conductivity," *Journal of Nuclear Materials*, vol. 462, pp. 289-295, 2015.
- [10] A. T. Nelson, "Prospects for additive manufacturing of nuclear fuel forms," *Progress in Nuclear Energy*, vol. 155, p. 104493, 2023.
- [11] H. S. Lee, D. S. Kim, D.-J. Kim, J. H. Yang, J.-H. Yoon, Y.-H. Koo and K. W. Song, "Numerical investigation of the thermal conductivity of UO₂ - Mo microplate fuel pellets to realize enhanced heat transfer in the fuel radial direction," *Journal of Nuclear Materials*, vol. 554, p. 153075, 2021.
- [12] J. P. Gorton, D. Schappel, A. T. Nelson and N. R. Brown, "Impact of uranium oxide (UO₂) fuel with molybdenum (Mo) inserts on pressurized water reactor performance and safety," *Journal of Nuclear Materials*, vol. 542, p. 152492, 2020.
- [13] P. G. Medvedev and R. D. Mariani, "Conductive inserts to reduce nuclear fuel temperature," *Journal of Nuclear Materials*, vol. 531, p. 151966, 2020.
- [14] B. Yan, R. Gao, P. Liu, P. Zhang and L. Cheng, "Optimization of thermal conductivity of UO₂-Mo composite with continuous Mo channel based on finite element method and machine learning," *International Journal of Heat and Mass Transfer*, vol. 159, p. 120067, 2020.
- [15] J. K. Fink, "Thermophysical properties of uranium dioxide," *Journal of Nuclear Materials*, vol. 279, pp. 1-18, 2000.
- [16] K. M. Paaren, P. Medvedev and R. Mariani, "Optimization of conductive fins to minimize UO₂ fuel temperature and radial temperature gradient," *Energies*, vol. 16, p. 2785, 2023.
- [17] J. H. Holland, "Genetic Algorithms," *Scientific American*, vol. 267, no. 1, pp. 66-73, 1992.
- [18] D. E. Goldberg, *Genetic Algorithms in Search, Optimization and Machine Learning*, Boston, MA: Addison-Wesley Longman Publishing Co., 1989.

- [19] S. Katoch, S. S. Chauhan and V. Kumar, "A review on genetic algorithm: past, present, and future," *Multimedia Tools and Applications*, vol. 80, pp. 8091-8126, 2021.
- [20] S. J. Louis and G. J. Rawlins, "Syntactic analysis of convergence in genetic algorithms," in *Foundations of Genetic Algorithms*, vol. 2, B. M. Spatz, Ed., San Mateo, CA, Morgan Kaufmann Publishers, Inc., 1993, pp. 141-151.
- [21] ANSYS, Inc., "ANSYS® Mechanical, Release 21.2," ANSYS, Inc., 2021.
- [22] D. D. Lanning, C. E. Beyer and K. J. Geelhood, "FRAPCON-3 Updates, Including Mixed-Oxide Fuel Properties," U.S. Nuclear Regulatory Commission, NUREG/CR-6534, Vol. 4, PNNL-11513, 2005.
- [23] CINDAS, LLC, "Global Benchmark for Critically Evaluated Materials Properties Data," 2023. [Online]. Available: <https://cindasdata.com/products/tpmd>.
- [24] O. Roeva, S. Fidanova and M. Paprzycki, "Influence of the Population Size on the Genetic Algorithm Performance in Case of Cultivation Process Modelling," in *2013 Federated Conference on Computer Science and Information Systems*, Krakow, Poland, 2013.
- [25] J. Arabas, Z. Michalewicz and J. Mulawka, "GAVaPS - a Genetic Algorithm with Varying Population Size," in *Proceedings of the First IEEE Conference on Evolutionary Computation*, Orlando, FL, USA, 1994.
- [26] J. Andre, P. Siarry and T. Dognon, "An improvement of the standard genetic algorithm fighting premature convergence in continuous optimization," *Advances in Engineering Software*, vol. 32, pp. 49-60, 2001.
- [27] C. W. Ahn and R. S. Ramakrishna, "Elitism-Based Compact Genetic Algorithms," *IEEE Transactions on Evolutionary Computation*, vol. 7, no. 4, pp. 367-385, 2003.
- [28] M. Srinivas and L. M. Patnaik, "Adaptive probabilities of crossover and mutation in genetic algorithms," *IEEE Transactions on Systems, Man, and Cybernetics*, vol. 24, no. 4, pp. 656-667, 1994.
- [29] W. Zhou and W. Zhou, "Enhanced thermal conductivity accident tolerant fuels for improved reactor safety - A comprehensive review," *Annals of Nuclear Energy*, vol. 119, pp. 66-86, 2018.
- [30] Z. Hashin and S. Shtrikman, "A variational approach to the theory of the effective magnetic permeability of multiphase materials," *Journal of Applied Physics*, vol. 33, no. 10, pp. 3125-3131, 1962.
- [31] K. A. Terrani and A. T. Nelson, "3D printing of additive structures for nuclear fuels". U.S. Patent 11,437,153, 2022.
- [32] F. Calignano, M. Lorusso, J. Pakkanen, F. Trevisan, E. P. Ambrosio, D. Manfredi and P. Fino, "Investigation of accuracy and dimensional limites of part produced by aluminum

alloy by selective laser melting," *The international Journal of Advanced Manufacturing*, vol. 88, pp. 451-458, 2017.

- [33] L. Kaserer, J. Braun, J. Stajkovic, K. H. Leitz, B. Tabernig, P. Singer, I. Letofsky-Papst, H. Kestler and G. Leichtfried, "Fully dense and crack free molybdenum manufactured by Selective Laser Melting through alloying with carbon," *International Journal of Refractory Metals and Hard Materials*, vol. 84, p. 105000, 2019.
- [34] C. Xu, B. Quinn, L. L. Lebel, D. Therriault and G. L'Espérance, "Multi-material direct ink writing (DIW) for complex 3D metallic structures with removable supports," *ACS Applied Materials & Interfaces*, vol. 11, pp. 8499-8506, 2019.
- [35] J. S. Pelz, N. Ku, W. T. Shoulders, M. A. Meyers and L. R. Vargas-Gonzalez, "Multi-material additive manufacturing of functionally graded carbide ceramics via active, in-line mixing," *Additive Manufacturing*, vol. 37, p. 101647, 2021.
- [36] D. Han and H. Lee, "Recent advances in multi-material additive manufacturing: methods and applications," *Current Opinion in Chemical Engineering*, vol. 28, pp. 158-166, 2020.

1
2
3